J. Biochem. 2010;147(1):53–61 doi:10.1093/jb/mvp143

JB THE JOURNAL OF BIOCHEMISTRY

Protruding masticatory (superfast) myosin heads from staggered thick filaments of dog jaw muscle revealed by X-ray diffraction

Received May 27, 2009; accepted August 27, 2009; published online September 16, 2009

Maki Yamaguchi[1,*], Shigeru Takemori[1], Masako Kimura[1], Yuichiro Tanishima[1,2], Tomoko Nakayoshi[1,2], Sumiko Kimura[3], Tetsuo Ohno[1], Naoto Yagi[4], Joseph F. Y. Hoh[5] and Yoshiki Umazume[1]

[1]Department of Molecular Physiology; [2]Department of Surgery, The Jikei University School of Medicine, Minato-ku, Tokyo, 105-8461; [3]Department of Biology, Faculty of Science, Chiba University, Inage-ku, Chiba, 263-8522; [4]Japan Synchrotron Radiation Research Institute, SPring-8, Sayo-cho, Sayo-gun, Hyogo, 679-5198, Japan; and [5]Discipline of Physiology and the Bosch Institute, F13, School of Medical Sciences, Sydney Medical School, The University of Sydney, NSW, 2006, Australia

*Maki Yamaguchi, Department of Molecular Physiology, The Jikei University School of Medicine, Minato-ku, Tokyo, 105-8461. Tel: +81-3-3433-1111, Fax: +81-3-3431-3826, E-mail: maki@jikei.ac.jp

To characterize the structure of jaw muscle fibres expressing masticatory (superfast) myosin, X-ray diffraction patterns of glycerinated fibres of dog *masseter* were compared with those of dog *tibialis anterior* in the relaxed state. Meridional reflections of *masseter* fibres were laterally broad, indicating that myosin filaments are staggered along the filament axis. Compared with *tibialis anterior* fibres, the peak of the first myosin layer line of *masseter* fibres was lower in intensity and shifted towards the meridian, while lattice spacings were larger at a similar sarcomere length. These suggest that the myosin heads of masticatory fibres are mobile, and tend to protrude from the filament shaft towards actin filaments. Lowering temperature or treating with *N*-phenylmaleimide shifted the peak of the first myosin layer line of *tibialis anterior* fibres towards the meridian and the resulting profile resembled that of *masseter* fibres. This suggests that the protruding mobile heads in the non-treated masticatory fibres are in the ATP-bound state. The increased population of weakly binding cross-bridges may contribute towards the high specific force of masticatory fibres during contraction. Electron micrographs confirmed the staggered alignment of thick filaments along the filament axis within sarcomeres of masticatory fibres, a feature that may confer efficient force development over a wide range of the sarcomere lengths.

Keywords: dog jaw muscle/kinetics/masseter myosin/synchrotron radiation/X-ray diffraction.

Abbreviations: MyBP-C, myosin binding protein C; MyHC, myosin heavy chain; PIPES, piperazin-1,4-bis(2-ethanesulfonic acid); NPM, N-phenylmaleimide

Masticatory (superfast) myosin is a distinct subclass (myosin IIM) of vertebrate striated myosin with ~70% homology of primary structure compared with limb fast myosin (*1*). This isoform is expressed in jaw-closing muscles of carnivorous lower vertebrates (*2*) and several orders of eutherians and most orders of marsupial mammals (*3*, *4*). Rowlerson and co-workers (*5*) first described this isoform, and showed that it has a 2- to 3-fold higher ATPase activity compared with that of limb fast myosin. From its high myosin ATPase activity and the fact that the time course of the isometric twitch of cat jaw muscle was much faster than that of the limb fast muscle (*6*), the label 'superfast' was applied to this myosin, based on the assumption that this myosin obeys Barany's relationship between ATPase activity and shortening velocity (*7*).

The unique property of muscle fibres associated with this myosin progressively emerged. Kato *et al.* (*8*) and Saeki *et al.* (*9*) measured Ca^{2+}-activated tension and ATPase activity of skinned fibres from cat muscles (*m. masseter* and *m. temporalis*) that express masticatory myosin. They found that normalized maximum tension and ATPase activity were considerably higher in masticatory fibres (130–190% for tension, 160–200% for ATPase) compared with limb fast fibres in the same animal. Their result indicated that 'tension cost' (ATPase activity/force output) of masticatory fibres was higher. They also showed that masticatory fibres exhibited remarkably faster tension recovery after a quick stretch, compared with fast or slow fibres (*8*), consistent with their faster twitch time course (*6*). Contrary to expectation, however, recent mechanical analysis of masticatory fibres revealed a shortening velocity intermediate between those of slow and fast limb fibres (*10*). Furthermore, stiffness measurement of isometrically contracting masticatory fibres over a range of frequencies indicated that the frequency at which stiffness drops to a minimum, f_{min}, which reflects the kinetic constants of cross-bridge cycling, is not higher than that of fast limb fibres (*11*). All of these observations show that masticatory myosin has quite different kinetics compared with other myosins, and does not obey Barany's relationship derived mainly from limb type myosins of various animal species. It is now obviously inappropriate to qualify this myosin as 'superfast', and 'masticatory' is used instead.

The attitude of myosin heads has an important influence on the kinetics of contraction in cardiac and skeletal muscles. In cardiac muscle, phosphorylation of myosin binding protein-C (MyBP-C) in thick filaments causes myosin heads to extend out towards thin

filaments, thereby increasing the probability of myosin heads forming weak attachments to thin filaments in the absence of activation (*12*, *13*). During β-adrenergic stimulation of cardiac muscle, MyBP-C phosphorylation enhances the cross-bridge attachment rate to compensate for the accelerated cross-bridge detachment rate due to troponin-I phosphorylation, which would otherwise reduce isometric force (*14*). In fast skeletal muscle, tetanically induced phosphorylation of myosin light chain-2 is associated with protrusion and deviation from the helical arrangement of myosin heads, leading to accelerated cross-bridge attachment and enhanced twitch force (*15*–*17*). As masticatory fibres express a unique isoforms of myosin heavy chain (MyHC) and light chains (*5*, *18*), as well as MyBP-C (*19*, *20*), there may well be structural characteristics in the thick filaments of masticatory fibres that contribute to their contractile properties.

In this study, we carried out X-ray diffraction experiments, as well as electron microscopy on relaxed glycerinated (skinned) fibres of dog *masseter* muscle, which express predominantly masticatory myosin, to detect possible structural features of the sarcomere, in particular, those of the thick filament that might be relevant to their unique mechanical properties. For comparison, dog *tibialis anterior* muscle, which expresses fast and slow myosins, was also studied.

Methods

Samples and solutions

M. masseter and *m. tibialis anterior* were dissected from dogs (Nosan Beagle, 13–17 kg) which were euthanized by overdose of isoflurane under an approval for animal experiments in Jikei University School of Medicine. Thin muscle strips with extracellular matrix, which is especially rich in *masseter* muscle, were chemically skinned for 3 h in skinning solution, which is prepared by including 0.2% triton X-100 in relaxing solution composed of Na_2ATP 4.7 mM, $Mg(methanesulfonate)_2$ 6.5 mM, EGTA 10 mM, K(methansulfonate) 55 mM, Na_2(phosphocreatine) 10 mM, creatine phosphokinase 140 U/ml, piperazin-1,4-*bis*(2-ethanesulfonic acid) (PIPES) 20 mM, at pH 7.0 (ionic strength: 0.2). After the skinning, the fibres were transferred to the relaxing solution mixed with an equal volume of glycerol and stored at −20°C. Just before the experiment, a fibre bundle of well-aligned 15–30 fibres forming a fascicle was carefully dissected from the strip as a specimen. In some experiments, fibre bundles were treated with *N*-phenylmaleimide (NPM) before obtaining X-ray diffraction patterns. NPM treatment selectively alkylates the sulfhydryl groups of the myosin head designated as SH1 and SH2 (*21*), which are conserved in masticatory myosin (*1*). The NPM treatment was carried out according to Xu *et al.* (*22*). Briefly, fibre bundles were reacted with NPM in the relaxing solution containing 0.1 mM NPM for 1 h. The reaction was terminated by returning the fibres to the relaxing solution with 5 mM DTT. No significant crosslink between other sarcomeric proteins was detected by SDS–PAGE of the fibres after the NPM treatment.

X-ray diffraction experiments

X-ray diffraction experiments were carried out at beam line 45XU in SPring8 (Hyogo, Japan). A fibre bundle was mounted tautly in a bath with both ends tied with silk monofilaments. The parallel arrangement of fibres within the *masseter* specimens seemed identical to that within the *tibialis anterior* specimens. Diffraction patterns were obtained in the relaxed state by perfusing specimens with the relaxing solution continuously at 20 and 5°C. Sarcomere length of the specimens was adjusted to the desired value ranged from 2.2 to 2.7 μm guided by laser diffraction. X-ray diffraction patterns were recorded using an imaging plate system (BAS 2500, Fuji Xerox). The X-ray wavelength was 0.09 nm and the specimen-to-detector distance was 1.8 m. Dithiothreitol (5 mM) and catalase (1000 U/ml) were added to the solutions in order to minimize tissue damage from free radicals that are produced by the X-rays (*23*).

Analysis of diffraction patterns

Each X-ray diffraction pattern was rotated around the beam centre by using the third-order myosin meridional reflections on either side of the equator as axis guides. After successive quadrant averaging, myosin first layer line and equatorial reflections were analysed.

The intensity within the range of 1/62.5–1/25.6 nm^{-1} along the meridional axis and 1/50–1/6.7 nm^{-1} along the equatorial axis was used for the analysis of myosin layer line. To extract the myosin component from the first layer line which is composed of myosin and actin components, the integrated intensity distribution along the meridional axis within the slice of 0.00103 nm^{-1} in the equatorial direction was separated into two gaussian distributions which have peaks at 1/42.9 and 1/36.5 nm^{-1}. The profile of the first myosin layer line was obtained by plotting the integrated intensity of the former distribution along the equatorial axis. The intensity of the first myosin layer line was expressed relative to the integrated intensity of the 1/5.9 nm^{-1} actin layer lines within the range of 1/4.8–1/6.9 nm^{-1} along the meridional axis and 1/50–1/6.7 nm^{-1} along the equatorial axis.

SDS–PAGE of myosin heavy chains (MyHCs) and connectin/titin

Skinned fibres prepared similarly to those used for the X-ray diffraction experiment were dissolved in SDS sample buffer, and heated for 3 min at 95°C. SDS–PAGE of MyHC was carried out in 8% gel according to the method of Talmadge and Roy (*24*) as modified by Hoh *et al.* (*6*). SDS–PAGE of connectin/titin was carried out according to the method of Laemmli (*25*), with 2.3–4% gradient polyacrylamide as the running gel [acrylamide: methylenebisacrylamide = 30 : 1.5 (w/w)]. The gels were stained for protein with Coomassie Brilliant Blue.

Electron microscopy

Fibre bundles from *masseter* and *tibialis anterior* muscles were tied to entomological pins under tension at 2.2 or 3.7 μm of sarcomere length before fixation to avoid shortening. Bundles were chemically fixed in a solution containing 2% glutaraldehyde and 100 mM sodium phosphate buffer (pH 7.4) overnight at 4°C. Tissue processing was completed by standard procedures for dehydration and Epon embedding. Thin longitudinal sections were stained with uranyl acetate and lead citrate. Electron micrographs were taken with H-7500 (operating voltage, 80 kV; Hitachi, Japan).

Results and discussion

SDS–PAGE of MyHCs

Figure 1 shows SDS–PAGE of MyHCs from fibre bundles of *masseter* and *tibialis anterior* muscles. The *tibialis anterior* sample (right) shows three bands, which may be identified as slow (I) type, fast IIx type and fast IIa type MyHCs, in the order of decreasing electrophoretic mobility, as previously shown for several mammalians by western blotting with monospecific antibodies (*26*). The dominant *tibialis anterior* MyHCs are fast (IIa) and slow (I). *Masseter* sample (left) shows two MyHC components: a weak slow (I) MyHC, which has the same mobility as that of *tibialis anterior* muscle and a prominent masticatory (IIM) type MyHC, which has a slightly slower mobility than the slow (I) MyHC, as in other mammals (*4*). The results confirmed that fibres used in this study contained the expected difference in MyHC composition.

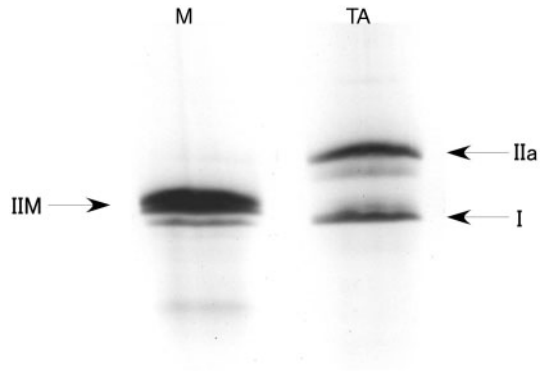

Fig. 1 SDS–PAGE of MyHCs in *masseter* and *tibialis anterior* fibres. Left gel: *masseter* fibres, showing a strong masticatory type (IIM) MyHC (arrowed) and a weak slow (I) MyHC. Right gel: *tibialis anterior* fibres, showing two strong MyHCs (arrowed; IIa, fast IIa type and I, slow type), with a weak fast IIx type MyHC in between.

General characteristics of X-ray diffraction patterns in the relaxed state

To compare the structural characteristics of the *masseter* and *tibialis anterior* muscles, we obtained X-ray diffraction patterns from bundles of chemically skinned fibres of these muscles at 20°C in the relaxed state. Representative two-dimensional diffraction patterns from these muscles are shown in Fig. 2. At a glance, some of the myosin layer lines of *masseter* fibres (upper panel) are weaker compared with *tibialis anterior* fibres (lower panel). As evidently observable with equatorial reflections, X-ray diffraction patterns from *masseter* fibres are slightly arced indicating that individual fibres within *masseter* bundles, or the population of thick and thin filaments in *masseter* fibres are misaligned with respect to each other. Since, as stated in the Methods section, the parallel alignment of the fibres within *masseter* specimens seemed identical to that within *tibialis anterior* specimens, we infer that misalignment at a subcellular level caused the arced feature. Besides the arc, meridional reflections arising from myosin heads at an order of $1/14.3\,nm^{-1}$ are laterally broad in *masseter* fibres. This feature suggests that thick filaments in *masseter* fibres are staggered in the axial direction, as confirmed by electron micrography described below.

Adequacy of ATP in fibre bundles to ensure the relaxed state

Because we used muscle bundles of 15–30 fibres, it is important to confirm whether the concentration of ATP at the core of the bundle was sufficient for the fibres to be in the relaxed state. We compared the X-ray diffraction patterns obtained in the standard solution with those obtained in a solution in which MgATP was increased from 4.7 to 5.9 mM and creatine phosphate from 10 to 32 mM, but found no evidence of rigor to relaxation change in the X-ray diffraction patterns of either *masseter* or *tibialis anterior* fibre bundles. This suggests that the unique characteristics of the *masseter* fibres found in this study

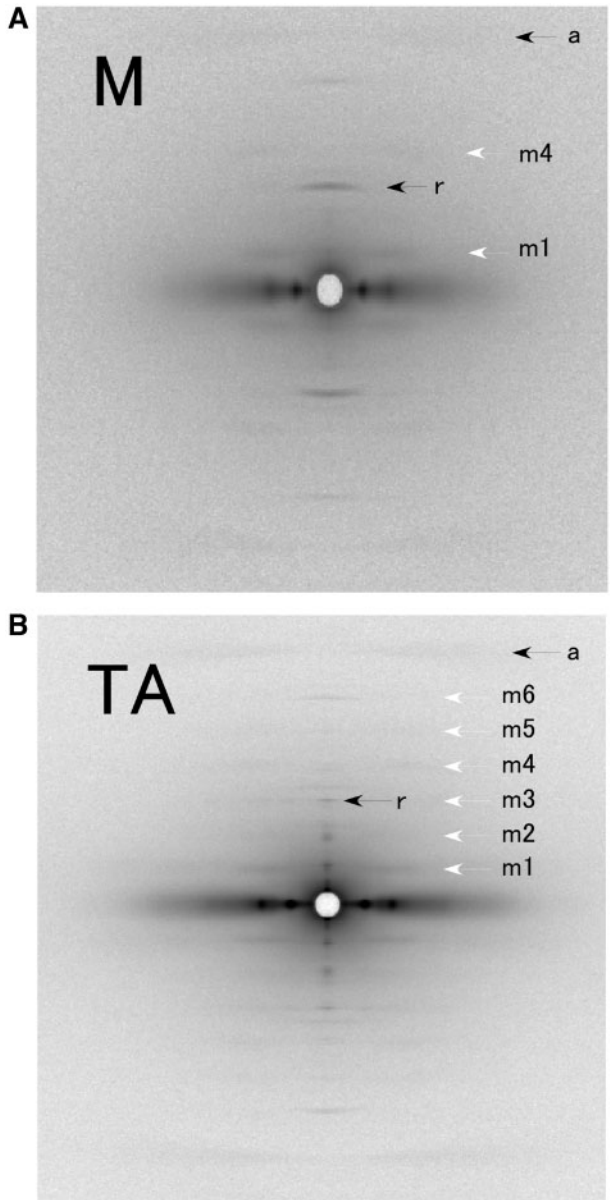

Fig. 2 X-ray diffraction patterns recorded from bundles of *masseter* (A) and *tibialis anterior* fibres (B) at 20°C. The arrows labelled *r* indicate the meridional reflection at $1/14.3\,nm^{-1}$ arising from myosin heads. The arrows labelled m1–m6 indicate layer lines arising from the thick filaments, and the arrows labelled a indicate layer lines at $1/5.9\,nm^{-1}$ arising from the thin filaments. The intensities are scaled to the integrated intensity of the layer line at $1/5.9\,nm^{-1}$ in each pattern.

can be attributed to the nature of the masticatory myosin in the relaxed state.

First myosin layer line at 20 and 5°C

Figure 3A shows the averaged relative intensity profiles of the first myosin layer lines ($1/42.9\,nm^{-1}$) along the equator for *masseter* and *tibialis anterior* fibres at 20°C in the relaxed state. The peak of the intensity profile from *masseter* fibres was lower, and its position was shifted towards the meridian compared with the corresponding features in *tibialis anterior* fibres. Since the peak position and the peak height of the first myosin layer line reflect the distribution of myosin

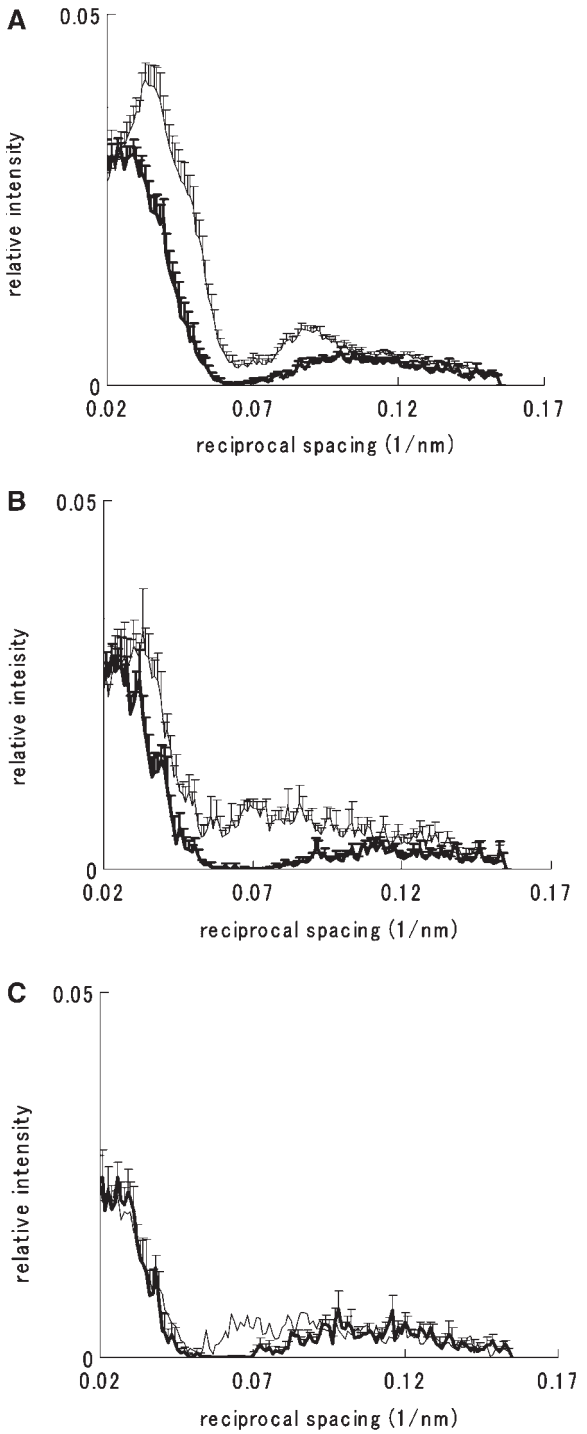

Fig. 3 Averaged intensity profiles of the first myosin layer lines (m1 in Fig. 2) along the equator obtained from bundles of *masseter* (thick line) and *tibialis anterior* (thin line) fibres. The intensities are scaled to the integrated intensity of the thin-filament associated layer line at 1/5.9 nm^{-1} (*a* in Fig. 2). Bars indicate a standard error of the mean (SE). (A) In relaxed state at 20°C. $n = 11$ for *masseter* fibres and 13 for *tibialis anterior* fibres. Peak intensity occurred at a reciprocal spacing of 0.026 nm^{-1} for *masseter* fibres and 0.034 nm^{-1} for *tibialis anterior* fibres. These values were obtained by least squares fit of gaussian distribution to the data from 0.02 to 0.06 nm^{-1} in reciprocal spacing. The estimated helical radius of the myosin heads are 25.7 nm for *masseter* fibres and 19.7 nm for *tibialis anterior* fibres. Averaged sarcomere lengths were 2.5 ± 0.04 μm (SE) for *masseter* fibres and 2.4 ± 0.05 μm (SE) for *tibialis anterior* fibres. (B) In relaxed state at 5°C. $n = 5$ for *masseter* fibres and 7 for *tibialis anterior* fibres. Peak intensity occurred at reciprocal spacings of 0.022 nm^{-1} for *masseter* fibres and 0.028 nm^{-1} for *tibialis anterior* fibres. These values were obtained by least squares fit of gaussian distribution to the data from 0.02 to 0.052 nm^{-1} in reciprocal spacing. The estimated helical radius of the myosin heads are 30.4 nm for *masseter* fibres and 23.9 nm for *tibialis anterior* fibres. Averaged sarcomere lengths were 2.6 ± 0.02 μm (SE) for *masseter* fibres and 2.5 ± 0.07 μm (SE) for *tibialis anterior* fibres. (C) After NPM treatment at 20°C. $n = 3$, and 2 for *masseter* (thick line) and *tibialis anterior* (thin line) fibres, respectively. The reciprocal spacing of the peak position was 0.024 nm^{-1} for both *masseter* and *tibialis anterior* fibres. This value was obtained by least squares fit of gaussian distribution to the data from 0.02 to 0.052 nm^{-1} in reciprocal spacing. The estimated helical radius of the myosin heads are 27.9 nm for both *masseter* and *tibialis anterior* fibres. Averaged sarcomere lengths were 2.5 μm for *masseter* fibres and 2.2 μm for *tibialis anterior* fibres.

heads around the backbone of thick filaments and the helical order of myosin heads, respectively (*27*), these results indicate that the myosin heads in *masseter* fibres protrude further away from the thick filaments and deviate from helical arrangement, compared with those in *tibialis anterior* fibres. This characteristic of *masseter* myosin heads is similar to that induced in fast skeletal muscle by phosphorylation of myosin light chain-2 referred to in the 'Introduction' section, and could be due to intrinsic differences in the myosin structure. In this connection, it is of interest that the amino acid sequence at the neck and hinge regions of masticatory MyHC shows considerable divergence relative to corresponding regions of other vertebrate MyHCs (H. Qin, M.K.H. Hsu and J.F.Y. Hoh, unpublished results). However, the protrusion of masticatory myosin heads may also be due to the expression of a masticatory fibre-specific MyBP-C isoform (*19*, *20*), since protrusion of the myosin heads can be brought about in cardiac muscle by phosphorylation of cardiac MyBP-C (*12*, *13*).

Figure 3B shows the averaged intensity profiles of the first myosin layer lines of *masseter* and *tibialis anterior* fibres at 5°C in the relaxed state. Compared with the intensity profile at 20°C, the profile of the *masseter* fibres at the lowered temperature was not significantly different, while that for the *tibialis anterior* fibres was substantially different: the main peak observed was reduced in height, and its position was shifted towards the meridian at 5°C. Theses effects of lowering the temperature on dog limb fibres are similar to those of rabbit fast fibres reported by previous workers (*28*, *29*). They attributed these changes in the rabbit fast fibres to a shift of equilibrium from M-ADP-Pi to M-ATP (where M denotes myosin) at the lowered temperature (*30*). In view of this, the possibility arises that the protrusion and deviation from the helical arrangement of myosin heads in *masseter* fibres at 20°C reflect a higher population of M-ATP heads than in *tibialis anterior* fibres at the same temperature. This possibility was tested by X-ray diffraction analysis of the fibres after NPM treatment.

First myosin layer lines after NPM treatment

NPM is an agent that inhibits myosin ATPase activity by trapping myosin at the M-ATP state by selectively alkylating the SH1 and SH2 of the myosin head (*21*). X-ray diffraction patterns from fibres in

the relaxed state after the NPM treatment were obtained at 20°C. After the treatment, the peak of the first myosin layer line of the *tibialis anterior* fibres was reduced in height and shifted towards the meridian, simulating the effect of lowered temperature (Fig. 3C). However, in the case of the *masseter* fibres, changes in position and amplitude of the main peak were small. As a result, NPM treatment of the *tibialis anterior* fibres, or lowering the temperature, made the diffraction pattern of the *tibialis anterior* fibres similar to that of the *masseter* fibres at 20°C. This suggests the idea that the protruding heads in the non-treated *masseter* fibres are in the M-ATP state.

Significance of protruding heads of masticatory myosin

The effect of the NPM treatment on the X-ray diffraction pattern of fast rabbit *psoas* muscle fibres in the relaxed state was examined by Xu *et al*. (*30*). They showed that NPM treatment decreased the intensity of the myosin first layer line, similarly to the effect of lowered temperature. In our study, NPM treatment also decreased the intensity of myosin first layer line in the dog *tibialis anterior* fibres, similarly to the effect of the lowered temperature on these fibres, but NPM treatment did not affect that of *masseter* fibres. Quantitative comparison of the observation of Xu *et al*. on the effects of NPM treatment on the first myosin layer line intensity with that of ours is not possible because they described the intensity after the NPM treatment as 'below detectable level'. However, our result is qualitatively consistent with theirs despite the difference in the muscle used. Thus, the effects of temperature and NPM treatment on *tibialis anterior* and *masseter* fibres observed in this study suggest that at 20°C the majority of the myosin heads in *masseter* fibres are in the M-ATP state in the relaxed state. This is supported by our biochemical observation that the size of the phosphate burst at 25°C measured by the malachite green method (*31*) was smaller for dog masticatory myosin [0.26 ± 0.11 Pi/myosin head, in mean ± standard error of the mean (SE)] than that for rabbit fast myosin [0.58 ± 0.09 Pi/myosin head, $P < 0.02$ by Student's *t*-test (Ohno and Yamaguchi, unpublished results)]. The smaller phosphate burst suggests that the population of ATP-bound head of masticatory myosin is larger than that of fast type myosin in the relaxed state at room temperature.

As pointed out by Xu and Gu (*22*, *32*), since the affinity of M-ATP for actin is considerably higher than that of M-ADP-Pi *in vitro* (*33*), it is likely that the protruding *masseter* M-ATP heads that are mobile and deviated from the helical arrangement, should have a much higher affinity for actin than the relatively static M-ADP-Pi wrapping around the filament shaft *in vivo*. Therefore, the abundance of M-ATP in masticatory fibres would favour the formation of weakly binding cross-bridges, thereby accelerating the flux of the rate limiting steps during the contraction cycle, including the phosphate cleavage step in the hydrolysis cycle. This would account for the higher ATPase activity of the *masseter* myosin. The short duration of twitch contraction of masticatory fibres compared with limb fast fibres implies that they have a faster rate of rise of tension. An accelerated rate of cross-bridge attachment in masticatory fibres could also help to explain this feature of masticatory muscle mechanics. Accelerated cross-bridge attachment, coupled with a moderate cross-bridge detachment rate, could also account for the high force feature and the increased 'tension cost' (ATPase activity/force output) reported in cat masticatory fibres (~120% of fast fibres). Thus the increased population of weakly binding cross-bridges may be the origin of some of the functional characteristics of masticatory fibres.

Outer peaks of the first myosin layer line profile

In the outer region of the first myosin layer line profile, other intensity peaks were observed in the *tibialis anterior* and *masseter* fibres (Fig. 3). In *tibialis anterior* fibres, a small but significant peak at $0.09\,nm^{-1}$ was observed at 20°C (Fig. 3A). Plausibly, this is the second peak of the Bessel function arising from the three-strand helical distribution of myosin heads (*27*). The peak is positioned further out than theoretically predicted (1.9 times of the first peak position). This is reasonably accounted for by the sampling effect of myofilament superlattice that would shift the first peak toward the meridian (*27*, *34*).

A broad peak at $0.11\,nm^{-1}$ was observed in *masseter* fibres (Fig. 3A–C). This is difficult to explain on the basis of a superlattice or Bessel function originating from a helix of myosin heads. A possible explanation for this peak is that the separation of the myosin and actin layer line components in the data analysis (see 'Methods' section) did not work well because of excessive overlap of these components due to the slight misalignment of the myofilaments conspicuously indicated by the arced equatorial reflections in *masseter* fibres.

To assign the origins of these peaks more conclusively, analysis of layer lines and reflections of higher orders based on atomic structures of the myosin molecules in *tibialis anterior* and *masseter* fibres would be necessary. In any event, absence of a significant peak at $0.09\,nm^{-1}$ in *masseter* fibres provides further evidence for their less ordered features.

Equatorial reflections

Remarkable differences between the *masseter* and *tibialis anterior* fibres were also observed in the equatorial reflections (Fig. 4). In the *masseter* fibres, the lattice spacing was larger than that of the *tibialis anterior* fibres at corresponding sarcomere lengths. We consider the larger spacing in *masseter* fibres compared with *tibialis anterior* fibres to be a consequence of sterical repulsion exerted by the protruding mobile myosin heads as discussed below.

Several factors are considered to affect the spacing of the thick filament lattice, depending on the state of muscle. In the rigor and contracting states, cross-bridges formed between the thick and thin filaments strongly affect the spacing. Even in the relaxed state, weakly binding cross-bridges formed at low-ionic

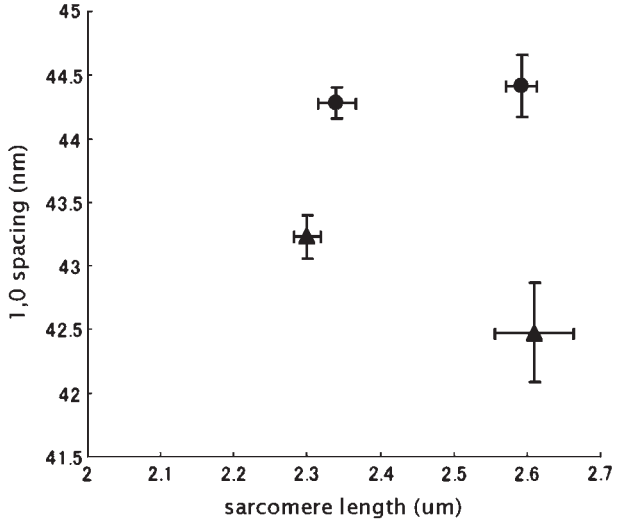

Fig. 4 The 1,0 lattice spacing plotted against the sarcomere length of bundles from *masseter* (filled circle) and *tibialis anterior* (filled triangle) fibres. The difference in lattice spacing between the *masseter* and *tibialis anterior* fibres was significant at both short ($P < 0.05$) and long sarcomere lengths ($P < 0.01$ by Student's *t*-tests). Bars indicate SE; $n = 5$ (*masseter*) and 6 (*tibialis anterior*) for fibres at the shorter sarcomere lengths, and $n = 13$ (*masseter*) and 10 (*tibialis anterior*) for fibres at the longer sarcomere lengths.

strength may affect the spacing (*35*). At a physiological ionic strength, myosin heads in ordinary skeletal muscle such as *tibialis anterior* play a minor role, if any, on the spacing in the relaxed state, but begin to resist compression beyond a critical filament spacing (*36*, *37*). The filament spacing of *masseter* fibres would be larger than that of a limb muscle, because the protruding mobile myosin heads are expected to exert steric repulsive force to expand the lattice even in uncompressed condition.

A similar expanding effect linked with protruding heads on thick filament lattice has been observed by Xu *et al*. for M-ATP heads in rabbit *psoas* muscle (*28*). Consistent correlation between myosin head protrusion and an increase in the lattice spacing was observed in the *tibialis anterior* with the lowered temperature and NPM treatment: that is, lowering temperature from 20 to 5°C increased the spacing of *tibialis anterior* fibres by 1.2 ± 0.5% (mean ± SE; paired analysis) but not the spacing in *masseter* fibres (−0.5 ± 0.5%), and NPM treatment diminished the difference in the lattice spacing between *tibialis anterior* and *masseter* fibres at 20°C (43.5 ± 0.88 nm in *masseter* fibres at the sarcomere length of 2.6 ± 0.05 μm, and 43.3 ± 1.16 nm in *tibialis anterior* fibres at the sarcomere length of 2.5 ± 0.07 μm).

Figure 4 also shows that at 20°C, the lattice of *masseter* fibres did not shrink as the sarcomere was stretched, whereas that of *tibialis anterior* fibres did. This not only supports the idea that steric repulsive force exerted by protruding mobile myosin heads strongly affects the spacing of myofilament lattice in *masseter* fibres, but also suggests that the heads are strong enough to overcome the compressive forces accompanying the sarcomere elongation of *masseter* fibres.

Fig. 5 SDS–PAGE of high molecular weight myofibrillar proteins in *masseter* and *tibialis anterior* fibres. Left gel; *masseter* fibres. Right gel; *tibialis anterior* fibres. Connectin/titin band is indicated by the upper arrow, while MyHC is indicated by the lower arrow.

SDS–PAGE of connectin/titin

Elastic filaments of the sarcomere comprising principally of connectin/titin have been discussed to be involved in lattice shrinkage with sarcomere elongation (*38*). From the lack of lattice shrinkage with sarcomere elongation in *masseter* fibres, one may consider the possibility that elastic filaments in *masseter* fibres are less abundant than in *tibialis anterior* fibres. To address this issue, we performed SDS-PAGE analysis of the specimens under the same condition as in the X-ray diffraction experiments to examine the amounts of connectin/titin or other large molecular weight proteins that may substitute for connectin/titin. The result (Fig. 5) suggests that the amount of connectin/titin relative to MyHC in *masseter* fibres was similar to that in *tibialis anterior* fibres. Therefore, the characteristics of the lattice spacing of *masseter* fibres are not attributable to the lack of elastic filaments. This, however, does not necessarily exclude the possibility that the structure and elasticity of sarcomeres in *masseter* fibres differ from those in *tibialis anterior* fibres, as discussed in the next subsection.

Electron micrography of masseter fibres

To compare the sarcomeric structure of *masseter* and *tibialis anterior* fibres, electron micrographs of longitudinal sections of these fibres were obtained (Fig. 6). The most prominent feature of *masseter* fibres is the disorder of their sarcomeric structure. The edges of the A-band (defined by the thick filaments) as well as those of the H-band (defined by the thin filaments) of the *masseter* fibres are irregular, implying either that there is inhomogeneity in the lengths of the thick and thin filaments, or that there is an axial stagger in the alignment of both thick and thin filaments. Furthermore, there is no discernible M-line in the *masseter* fibres, as was reported in cat masticatory fibres (*5*) in contrast with dense M-lines in the *tibialis anterior* fibres. These were essential features of *masseter* fibres irrespective of the sarcomere length (2.2 and 3.7 μm). The lack of a dense M-line suggests a weak connection between thick filaments in the lateral direction as reported in slow fibres in some mammalian species (*39*, *40*). This may well be the reason of the axial stagger of thick filaments in the *masseter* sarcomere. Thus, the elastic compliance of the *masseter* sarcomere is likely to be larger than that of

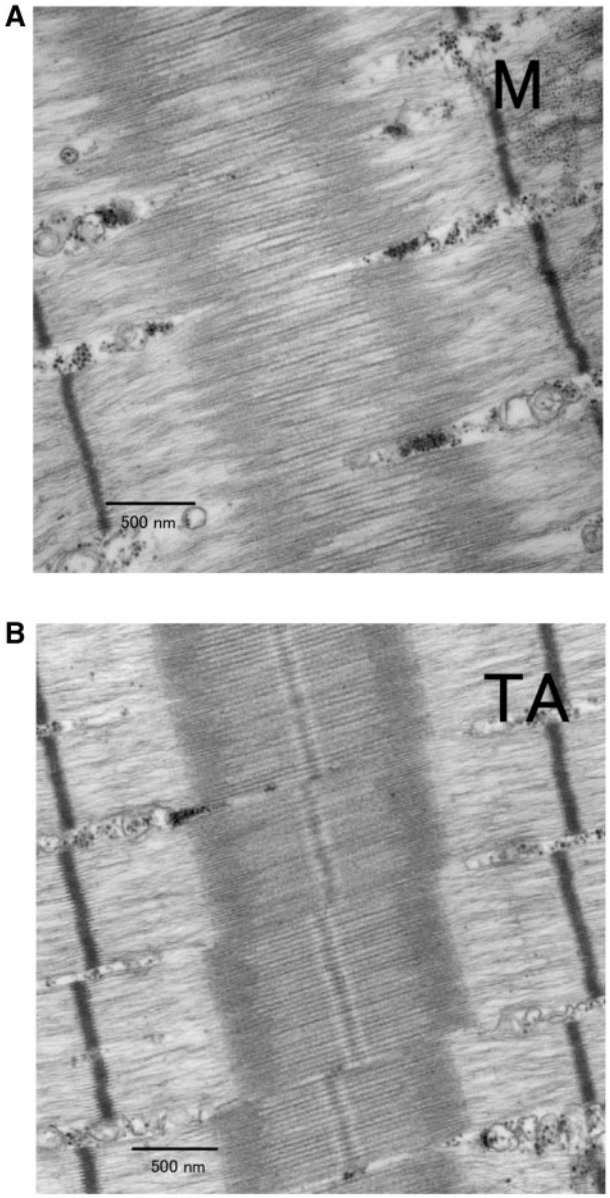

Fig. 6 Electron micrographs of longitudinal sections of *masseter* (A) and *tibialis anterior* (B) fibres. Sarcomere length of both specimens is 3.7 μm.

the *tibialis anterior* sarcomere. Note that axial stagger of the *masseter* thick filaments is consistent with the extended feature of the meridional reflections in the X-ray diffraction pattern of *masseter* fibres referred to earlier.

The elastic compliance is thought to allow a wider range of overlap between the neighbouring thick and thin filaments within a sarcomere. This would favour a stable tension development by suppressing the sarcomere damage especially at the descending limb of the length-tension curve where sarcomere instability likely occurs (*41*). Also, the elastic axial dislocation of each thick filament in a sarcomere can reinforce total (active plus passive) force because the axial deviation allows the individual thick filament to find another steady state with higher force where the two sides of the thick filament differ in overlap with thin filaments but total force is balanced (*41*).

In *masseter* muscle tissue, fibre fascicles run in various directions in rich extracellular matrices to realize complex motion of biting and mastication, and therefore are supposed to exert force at various sarcomere lengths. Thus the elastic sarcomeres of the masticatory fibres as well as the rich extracellular matrix would be a consequence of adaptation of the muscle to work efficiently over a wider range of sarcomere lengths.

Conclusion

In summary, our X-ray diffraction study suggests that the myosin heads of masticatory fibres are mobile, and tend to protrude from the filament shaft towards actin filaments. Analysis of the effects of a decrease in temperature and exposure to NPM on diffraction patterns suggests that the protruding and mobile masticatory myosin heads are in the ATP-bound state. X-ray diffraction as well as electron microscopy also showed axial stagger of the thick filaments with no discernible M-line, suggesting that masticatory fibres have a highly compliant sarcomere structure. These structural features may underlie the high specific force and ATPase activity of masticatory fibres.

Acknowledgements

The authors are grateful to Dr Jun Man for the MyHC analysis and to Dr Hiroyuki Sasaki and Ms. Emi Kikuchi for taking the electron micrographs. They also thank Dr Tetsuro Fujisawa and Dr Shinji Miyagawa for their help in the X-ray diffraction experiments. The X-ray diffraction experiments were performed at the BL45XU in SPring8 with the approval by Program Review Committee of the Japan Synchrotron Radiation Research Institute (JASRI) (proposal No. 2002B0493-NL-np, 2004B0781-NL2a-np).

Funding
The Jikei University Research Fund.

Conflict of interest
None declared.

References

1. Qin, H., Hsu, M.K.H., Morris, B.J., and Hoh, J.F.Y. (2002) Distinct subclass of mammalian striated myosins: structure and molecular evolution of ''superfast'' or masticatory myosin heavy chain. *J. Mol. Evol.* **55**, 544–552.
2. Hoh, J.F.Y., Lim, J.H.Y., Kang, L.D.H., and Lucas, C.A. (2001) Expression of superfast myosin in the jaw-closing muscles of Crocodylus porosus in *Crocodilian Biology and Evolution* (Grigg G.C., Seebacher F., and Franklin C.E., eds.), pp. 156–164, Surrey Beatty & Sons, Chipping Norton.
3. Hoh, J.F.Y. (2002) ''Superfast'' or masticatory myosin and the evolution of jaw-closing muscles of vertebrates. *J. Exp. Biol.* **205**, 2203–2210.
4. Hoh, J.F.Y., Kang, L.H., Sieber, L.G., Lim, J.H., and Zhong, W.W. (2006) Myosin isoforms and fiber types in jaw-closing muscles of Australian marsupials. *J. Comp. Physiol. [B]* **176**, 685–695.
5. Rowlerson, A., Pope, B., Murray, J., Whalen, R.B., and Weeds, A.G. (1981) A novel myosin present in cat jaw-closing muscles. *J. Muscle Res. and Cell Motil.* **2**, 415–438.

6. Taylor, A., Cody, F.W.J., and Bosley, M.A. (1973) Histochemical and mechanical properties of the jaw muscles of the cat. *Exp. Neurol.* **38**, 99–109.
7. Barany, M. (1967) ATPase activity of myosin correlated with speed of muscle shortening. *J. Gen. Physiol.* **50 (Suppl.)**, 197–218.
8. Kato, C., Saeki, Y., and Yanagisawa, K. (1985) Ca^{2+} sensitivities and transient tension responses to step-length stretches in feline mechanically stripped single-fibre jaw-muscle preparations. *Archs. Oral Biol.* **30**, 429–432.
9. Saeki, Y., Kato, C., Satomi, M., and Yanagisawa, K. (1987) ATPase activity and tension development in mechanically-skinned feline jaw muscle. *Archs. oral Biol.* **32**, 207–210.
10. Toniolo, L., Cancellara, P., Maccatrozzo, L., Patruno, M., Mascarello, F., and Reggiani, C. (2008) Masticatory myosin unveiled: first determination of contractile parameters of muscle fibers from carnivore jaw muscles. *Am. J. Physiol.* **295**, C1535–1542.
11. Hoh, J.F.Y., Li, Z.B., Qin, H., Hsu, M.K.H., and Rossmanith, G.H. (2007) Cross-bridge kinetics of fast and slow fibers of cat jaw and limb muscles: correlations with myosin subunit composition. *J. Muscle Res. Cell Motil.* **28**, 329–341.
12. Weisberg, A. and Winegrad, S. (1996) Alteration of myosin cross bridges by phosphorylation of myosin-binding protein C in cardiac muscle. *Proc. Natl. Acad. Sci. USA* **93**, 8999–9003.
13. Levine, R., Weisberg, A., Kulikovskaya, I., McClellan, G., and Winegrad, S. (2001) Multiple structures of thick filaments in resting cardiac muscle and their influence on cross-bridge interactions. *Biophys. J.* **81**, 1070–1082.
14. Turnbull, L., Hoh, J.F.Y., Ludowyke, R.I., and Rossmanith, G.H. (2002) Troponin-I phosphorylation enhances crossbridge kinetics during beta-adrenergic stimulation in rat cardiac tissue. *J. Physiol.* **542**, 911–920.
15. Hoh, J.F.Y., Yamaguchi, M., Kimura, M., Takemori, S., and Yagi, N. (2005) X-ray diffraction analysis of the effects of myosin chain-2 phosphorylation on the structure of fast skeletal muscle fibres. *Proc. Aust. Physiol. Soc.* **36**, 116P.
16. Metzger, J.M., Greaser, M.L., and Moss, R.L. (1989) Variations in cross-bridge attachment rate and tension with phosphorylation of myosin in mammalian skinned skeletal muscle fibers. Implications for twitch potentiation in intact muscle. *J. Gen. Physiol.* **93**, 855–883.
17. Levine, R.J., Kensler, R.W., Yang, Z., Stull, J.T., and Sweeney, H.L. (1996) Myosin light chain phosphorylation affects the structure of rabbit skeletal muscle thick filaments. *Biophys. J.* **71**, 898–907.
18. Qin, H., Morris, B.J., and Hoh, J.F.Y. (2004) Isolation and structure of cat superfast myosin light chain-2 cDNA and evidence for the identity of its human homologue. *Biochem. Biophys. Res. Commun.* **200**, 1277–1282.
19. Hoh, J.F.Y., Hughes, S., Kang, L.H.D., Rughani, A., and Qin, H. (1993) The biology of cat jaw-closing muscle cells. *J. Comp-Assist. Microsc.* **5**, 65–70.
20. Wu, X., Li, Z.F., Brooks, R., Komives, E.A., Torpey, J.W., Engvall, E., Gonias, S.L., and Shelton, G.D. (2007) Autoantibodies in canine masticatory muscle myositis recognize a novel myosin binding protein-C family member. *J. Immunol.* **179**, 4939–4944.
21. Barnett, V.A., Ehrlich, A., and Schoenberg, M. (1992) Formation of ATP-insensitive weakly-binding cross-bridges in single rabbit psoas fibers by treatment with phenylmaleimide or para-phenylenedimaleimide. *Biophys. J.* **61**, 358–367.
22. Xu, S., Gu, J., Melvin, G., and Yu, L.C. (2002) Structural characterization of weakly attached cross-bridges in the A-M-ATP state in permiabilized rabbit psoas muscle. *Biophys. J.* **82**, 2111–2122.
23. Kraft, K., Xu, S., Brenner, B., and Yu, L.C. (1999) The effect of thin filament activation on the attachment of weak binding cross-bridges: a two-dimensional X-ray diffraction study on single muscle fibers. *Biophys. J.* **76**, 1494–1513.
24. Talmadge, R.J. and Roy, R.R. (1993) Electrophoretic separation of rat skeletal muscle myosin heavy-chain isoforms. *J. Appl. Physiol.* **75**, 2337–2340.
25. Leammli, U.K. (1970) Cleavage of structural proteins during the assembly of the head of bacteriophage T4. *Nature* **227**, 680–685.
26. Lucas, C.A., Kang, L.H., and Hoh, J.F.Y. (2000) Monospecific antibodies against the three mammalian fast limb myosin heavy chains. *Biochem. Biophys. Res. Commun.* **272**, 303–308.
27. Haselgrove, J.C. (1980) A model of myosin cross-bridge structure consistent with the low-angle X-ray diffraction pattern of vertebrate muscle. *J. Muscle Res. and Cell Motil.* **1**, 177–191.
28. Xu, S., Malinchik, S., Gilroy, D., Kraft, Th., Brenner, B., and Yu, L.C. (1997) X-ray diffraction studies of cross-bridges weakly bound to actin in relaxed skinned fibers of rabbit psoas muscle. *Biophys. J.* **73**, 2292–2303.
29. Malinchik, S., Xu, S., and Yu, L.C. (1997) Temperature-induced structural changes in the myosin thick filament of skinned rabbit psoas muscle. *Biophys. J.* **73**, 2304–2312.
30. Xu, S., Gu, J., Rhodes, T., Belknap, B., Rosenbaum, G., Offer, G., White, H., and Yu, L.C. (1999) The M-ADP-Pi state is required for helical order in the thick filaments of skeletal muscle. *Biophys. J.* **77**, 2665–2676.
31. Kodama, T., Fukui, K., and Kometani, K. (1986) The initial phosphate burst in ATP hydrolysis by myosin and subfragment-1 as studied by a modified malachite green method for determination of inorganic phosphate. *J. Biochem.* **99**, 1465–1472.
32. Gu, J., Xu, S., and Yu, L.C. (2002) A model of cross-bridge attachment to actin in the A-M-ATP state based on X-ray diffraction from permeabilized rabbit psoas muscle. *Biophys. J.* **82**, 2123–2133.
33. White, H.D., Belknap, B, and Webb, M.R. (1997) Kinetics of nucleotide triphosphate cleavage and phosphate release steps by associated rabbit skeletal actomyosin, measured using a novel fluorescent probe for phosphate. *Biochemistry* **36**, 11828–11836.
34. Luther, P.K., Squire, J.M., and Forey, P.L. (1996) Evolution of myosin filament arrangements in vertebrate skeletal muscle. *J. Morphology* **229**, 325–335.
35. Umazume, Y., Onodera, S., and Higuchi, H. (1986) Width and lattice spacing in radially compressed frog skinned muscle fibres at various pH values, magnesium ion concentrations and ionic strengths. *J. Muscle Res. Cell Motil.* **7**, 251–258.
36. Umazume, Y., Higuchi, H., and Takemori, S. (1991) Myosin heads contact with thin filaments in compressed relaxed skinned fibres of frog skeletal muscle. *J. Muscle Res. Cell Motil.* **12**, 466–471.
37. Kimura, M. and Takemori, S. (2008) CH2-units on (Poly)-ethylene glycol radially dehydrate cytoplasm of resting skinned skeletal muscle. *J. Biochem.* **143**, 841–847.
38. Higuchi, H. and Umazume, Y. (1985) Localization of the parallel elastic components in frog skinned muscle fibers

studied by the dissociation of the A-and I-bands. *Biophys. J.* **48**, 137–147.
39. Agarkova, I., Schoenauer, R., Ehler, E., and Perriard, J.C. (2004) The molecular composition of the sarcomeric M-band correlates with muscle fiber type. *Eur. J. Cell Biol.* **83**, 193–204.
40. Agarkova, I., Ehler, E., Lange, S., Schoenauer, R., and Perriard, J.C. (2003) M-band: a safeguard for sarcomere stability? *J. Muscle Res. Cell Motil.* **24**, 191–203.
41. Allen, D.G. (2001) Eccentric muscle damage: mechanisms of early reduction of force. *Acta Physiol. Scand.* **171**, 311–319.